Journal of Materials Chemistry A

Accepted Manuscript

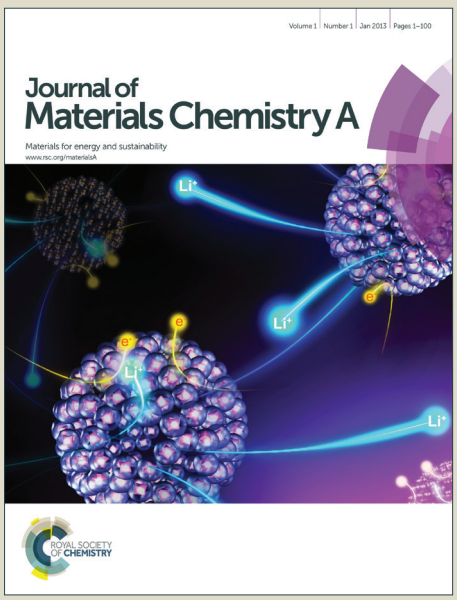

ROYAL SOCIETY OF CHEMISTRY

www.rsc.org/materialsA

Journal of Materials Chemistry A
CREATED USING THE RSC LaTeX PCCP ARTICLE TEMPLATE – SEE www.rsc.org/electronicfiles FOR DETAILS
PAPER
www.rsc.org/ees | Energy & Environmental Science

Highly efficient, flexible, indium-free perovskite solar cells employing metallic substrates†

Joel Troughton,[a] Daniel Bryant,[ac] Konrad Wojciechowski,[b] Matthew J. Carnie,[a] Henry Snaith,[b] David A. Worsley[a] and Trystan M. Watson,*[a]

Received Xth XXXXXXXXXX 20XX, Accepted Xth XXXXXXXXX 20XX
First published on the web Xth XXXXXXXXXX 200X
DOI: 10.1039/b000000x

Flexible perovskite solar cells with power conversion efficiencies of up to 10.3% have been prepared using titanium foil as an electrode substrate. Our method uses an indium-free transparent counter electrode which allows device performance to remain high despite repeated bending, making it suitable for roll-to-roll processing

During the short time since they were first used to make a functioning photovoltaic device, organic-inorganic lead halide perovskite solar cells have garnered much interest as promising light harvesters for highly efficient photovoltaic devices. Kojima *et al.*[1] first presented research into such materials for use in solar cells in 2009 following a liquid electrolyte based dye-sensitised solar cell (DSSC) configuration. Advances followed in 2012 whereby a solid hole transporter was used rather than a liquid electrolyte leading to greater stability and higher overall performance.[2,3] Since then, perovskite solar cells have achieved certified power conversion efficiencies (PCEs) in excess of 20%.[4] In addition to these high efficiencies, the technology has also shown great promise in terms of material availability, cost and ease of processing.[5,6] Several new methods for depositing the perovskite film have emerged including, vacuum deposition[7], vapour-assisted processing[8], sequential deposition of the organic and inorganic components[9], spray-coating[10] and co-deposition of perovskite and mesoporous scaffold.[11] These methods enable many routes to process the perovskite film on a variety of substrates with varying thermal requirements.

Typically perovskite solar cells are fabricated on fluorine doped tin oxide (FTO) coated glass as a working electrode substrate. Whilst this material provides excellent thermal and mechanical stability, the bulk and inflexibility associated with glass means roll-to-roll production is not possible. Recently, there have been developments in using ITO (tin doped indium oxide) coated polyethylene terephthalate (PET) as a substrate for perovskite solar cells as well as flexible fibre devices based on carbon nanotubes.[12–19] Inverted device architectures have demonstrated high efficiencies on ITO/PET substrates where instead of a compact TiO_2 electron acceptor layer, a fully organic PCBM film is used,[13,18] further enabling low-temperature fabrication of devices. Devices employing compact TiO_2 layers have reported excellent performance stability after several mechanical bending cycles, with efficiencies dropping as little as 7% below the original value.[17] In fact,

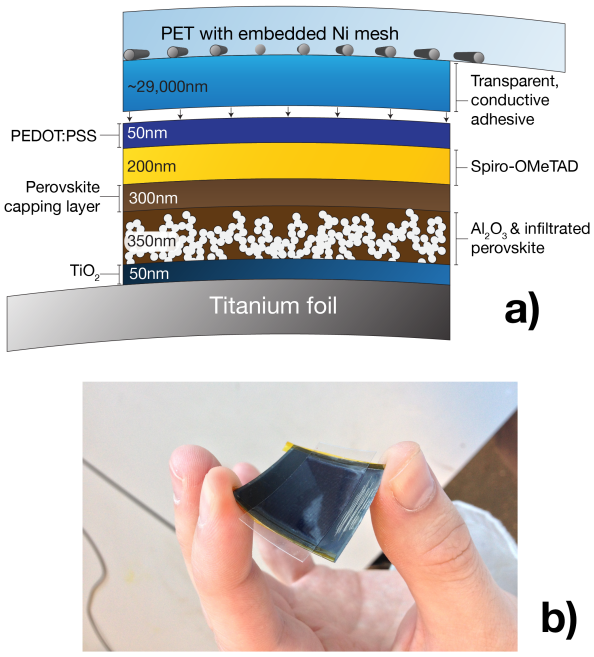

Fig. 1 (a) A schematic representation of a metal mounted perovskite solar cell and associated target layer thicknesses. (b) A photograph of a flexible perovskite solar cell on titanium foil.

† Electronic Supplementary Information (ESI) available: [details of any supplementary information available should be included here]. See DOI: 10.1039/b000000x/

[a] *SPECIFIC - College of Engineering, Swansea University, Singleton Park, Swansea, SA2 8PP, UK. Fax: XX XXXX XXXX; Tel: XX XXXX XXXX; E-mail: t.m.watson@swansea.ac.uk*
[b] *Photovoltaic and Optoelectronic Device Group, Department of Physics, Oxford University, UK*
[c] *Department of Chemistry, Imperial College London, UK*

Kim *et al.* showed that the degradation of the device performance by bending was a result of crack formation in the ITO layer rather than the TiO_2 electron selective layer. As an alternative to ITO/PET metallic foils combine greater mechanical and thermal stability, low material cost and superior electrical conductivity. Flexible metal foil based dye-sensitised solar cells (DSCs) were first demonstrated in 2006 by Ito *et al.*[20] and have garnered considerable attention from both academia and industry. These metal foil DSSCs are, in fact, currently manufactured by G24 Power in the UK on a commercial scale for consumer electronics. In these DCCSs, a PET/ITO counter-electrode above an electrolyte-filled cavity is used, however, the solid-state nature of modern perovskite solar cells requires a different approach.

In this work, we present flexible perovskite solar cells using commercially available titanium foil as a substrate onto which the device layers are deposited. For the counter-electrode, we use a transparent, conductive adhesive (TCA) coated laminate prepared *ex-situ* as demonstrated previously.[21] This counter-electrode eschews the ITO coating in favour of an electrodeposited nickel grid which is both cheaper at-scale and more mechanically robust in comparison. We report a PCE of 10.3% for a flexible, ITO-free perovskite solar cell using 150 µm thick titanium metal foil as a working electrode substrate. We explore the implications of various conductive interlayer thicknesses and mechanical bending on device performance. We also examine the implications of thermally grown electron collection layers (TiO_2) produced by heating the titanium substrate in air.

A schematic diagram of the metal foil cell's architecture is shown in Fig. 1(a), with a photograph of a larger device shown in Fig 1(b). The transparent counter-electrode is prepared *ex-situ* and laminated to the cell using light finger pressure. The tack quality is provided by an adhesive within the transparent laminate.[21]

Solar cells were prepared on 150 µm thick titanium foil which was polished and cleaned in alcohol before undergoing an oxygen plasma treatment. A compact layer of TiO_2 was deposited by spin coating and sintered for 2 minutes at 50 °C. Next, an insulating scaffold of Al_2O_3 nanoparticles was deposited and dried as described elsewhere.[22] On top of this, a $CH_3NH_3PbI_{3-x}Cl_x$ precursor solution was deposited by spin-coating and heated for 85 minutes at 100 °C, followed by 10 minutes at 120 °C in order to promote the growth of uniform micron-sized perovskite crystal domains. A solution containing 2,2',7,7'-tetrakis[N,N-di(4-methoxyphenyl)amino]-9,9'-spirobifluorene (spiro-OMeTAD), 4-*tert*-butylpyridine (tBP), bis(trifluoromethane)sulfonimide lithium salt (Li-TFSI) and vanadium pentoxide (V_2O_5) was spin-coated onto the perovskite films to form a hole-transport layer (HTL). The addition of V_2O_5 in the HTL serves to rapidly oxidise the Li-TFSI in seconds rather than the days normally required in order to reach peak conductivity.[23] An early comparative study of the V_2O_5-doped HTM against Li-TFSI and tBP-only doped HTL is shown in the ESI: Devices were tested within 2 hours of HTL deposition, giving the layer little time to dope in the presence of air. This brief study demonstrated that V_2O_5-doped spiro-OMeTAD yields significantly higher fill factors as well as reduces inter-cell variation compared to comparable devices with no V_2O_5. Next, poly(3,4-ethyl- enedioxythiophene):poly(styrenesulfonic acid) (PEDOT:PSS) diluted in 2-propanol was spray deposited onto the HTL and dried at 50 °C. *Ex-situ*, a flexible counter-electrode laminate was prepared by doctor blading a mixture of PEDOT:PSS and pressure sensitive adhesive onto a PET film embedded with a Ni grid. This film was then cured at 60 °C for 15 minutes, followed by 120 °C for 5 minutes before consolidation with the metal foil electrodes. Full details of device fabrication and characterisation are provided in the ESI†.

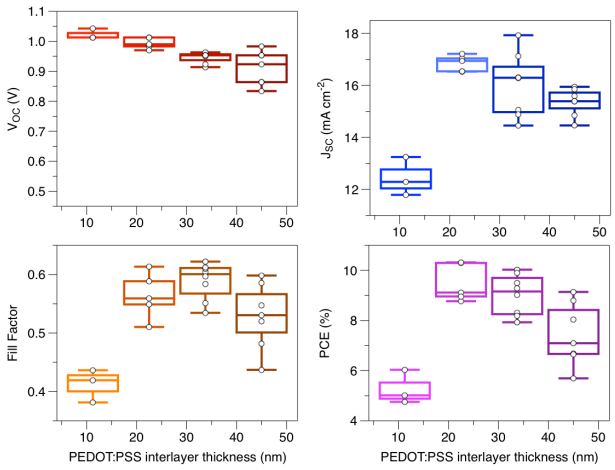

Fig. 2 Statistical analysis of Current-Voltage data with varying PEDOT:PSS interlayer thicknesses.

We found the largest variations in device performance were as a result of the thickness of the PEDOT:PSS interlayer spray-deposited onto the HTL as illustrated in Fig. 2. This conductive interlayer plays a critical role in transporting charge from the HTL to the small "islands" of PEDOT:PSS within the TCA. Since the TCA contains only around 1.75% PEDOT:PSS, with the rest being dielectric adhesive material, only a small proportion of the film would be able to transfer charge to the HTL in the absence of a conductive interlayer. These conductive outcrops within the TCA have previously been found to lie 200-300 nm apart[21], imposing severe current and fill factor limitations when combined directly with spiro-OMeTAD's low conductivity (2×10^{-5} S cm^{-2})[24]. The PEDOT:PSS interlayer mitigates this issue by providing a conductive lateral pathway to collect charges from the HTL and

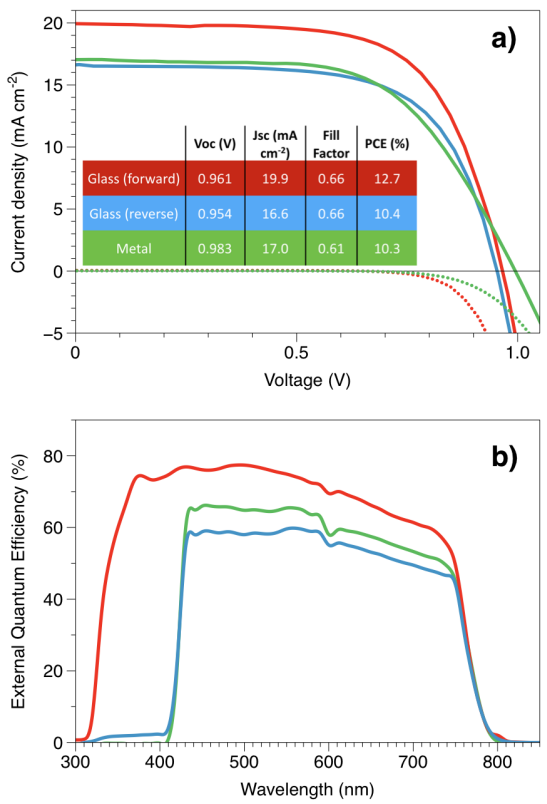

Fig. 3 Characterisation of highest performing metal and glass substrate solar cells. (a) Photocurrent density *versus* voltage measurements at 100 mW cm, 0.248 cm^2 active area. (b) External quantum efficiency spectra of cells. "Forward" measurements indicate illumination through the working electrode whereas "Reverse" indicates illumination through the counter electrode.

transport them to conductive sites within the TCA material, whereupon they are transferred to a highly conductive "highway" in the form of the Ni grid embedded within the PET film. In fact, this conductive interlayer is so effective it can actually draw charge from areas beyond those covered by the counter electrode, making effective active area masking especially important in order to obtain accurate photocurrent measurements.

Fig. 2 shows a sharp increase in both J_{SC} and fill factor as the PEDOT:PSS layer is increased from 11 nm to 22 nm , this indicates a critical threshold required to create a continuous layer by spray deposition. It stands to reason that layers below this thickness threshold are discrete, isolated islands of PEDOT:PSS owing to the small droplets of liquid generated by the spray gun. Low current is a result of this incomplete HTL-to-TCA contact laterally across the cell's surface. Fill factor also suffers as a result of this lower charge extraction capacity. There is also a trend towards decreasing V_{OC} with interlayer thickness which we have attributed to degradation of the Spiro-OMeTAD caused by the small amount of water in the PEDOT:PSS interlayer. The layer thickness is determined by number of spray passes and so a thicker layer is exposed to more water leading to increased degradation. At PEDOT:PSS thicknesses in excess of 22 nm, overall efficiency is reduced on account of dropping J_{SC}: This is a result of light attenuation by a thicker layer of material as the cell is illuminated through the TCA, PEDOT:PSS interlayer and HTL.

Current density versus voltage curves as well as EQE spectra are shown for champion devices in Fig. 3. A control specimen fabricated on FTO glass (7Ω sq^{-1}, Pilkington) in place of titanium foil is also shown. Since this control device may be illuminated through both the working electrode (glass, denoted as "forward") and counter electrode (PET/TCA, denoted as "reverse"), both illumination directions are shown. It is apparent that both reverse-illuminated glass and metal substrate cells suffer a substantial J_{SC} loss compared to a forward-illuminated glass device, previously observed in reverse illuminated DSSCs.[25] The EQE spectra in Fig.3(b) displays a severe cut-off at wavelengths below 400 nm, which is mainly attributed to highly effective ultraviolet filtering by the spiro-OMeTAD layer although the PET/TCA film as well as the PEDOT:PSS interlayer also play roles in this attenuation. A layer-by-layer transmission spectra is shown in the ESI† which verifies the origin of these losses as due to light attenuation. There is a slight increase in J_{SC} in the metal substrate device compared to the reverse-illuminated glass control which we attribute to a small degree of back reflection by the metallic substrate, yielding a light harvesting improvement not present in glass devices. A reflectance comparison is shown in the ESI† which shows an increase in reflection of up to 80% in the visible region of the spectrum in the case of titanium foil compared to c-TiO_2 coated FTO glass.

Bend cycle testing was also performed on devices: In this test, a cell was repeatedly manually deformed around a circular mould with a radius of 5 cm at a frequency of 1 Hz. The results of this test can be seen in the ESI†; after 200 bend cycles, the device's PCE was found to have dropped by less than 7%, mainly as a result of fill factor degradation which we attribute to cracking and delamination of the PEDOT:PSS/TCA interface within the cell. V_{OC} and J_{SC} remained remarkably consistent over the course of this test, proving that both the compact-TiO_2 and perovskite layers remain intact during mechanical deformation. This performance stability with deformation demonstrates the suitability of perovskite solar cells on metal foils for roll-to-roll production, where the bend radius is likely to be much larger, and so, less severe, than the 5 cm used in this experiment.

A selection of devices were measured using transient photovoltage (TPV) decay experiments, using the apparatus and

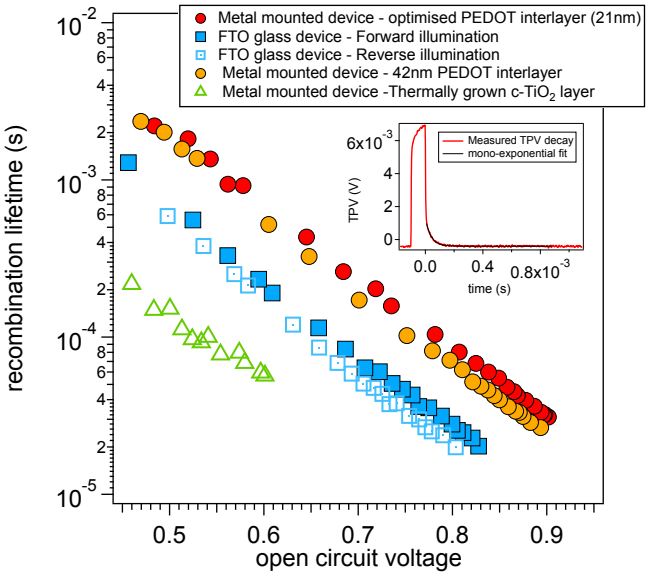

Fig. 4 Recombination lifetimes, measured by transient photovoltage decay, of a selection of metal and glass mounted devices

methods outlined by Barnes *et al.*[26] We observed that metal and glass mounted devices incorporating the flexible TCA electrode exhibit different TPV decay behaviours than those devices with evaporated Au contacts. In previous TPV experiments using Au evaporated counter electrodes we have identified multi-exponential decays indicating the possibility of more than one recombination process[27]. Conversely we have found that TCA-laminate devices exhibit almost exclusively mono-exponential decays (see Fig. 4) even though the transient photovoltage, ΔV was of a similar value ($\sim$10 mV) when measuring both types of device architectures. This behaviour is as yet, unexplained and is the focus of ongoing research. The mono-exponential decay however, does have an advantage in that the TPV decays are simple to model using a 1st-order exponential decay function delivering a single time-constant. Fig. 4 shows the TPV decay data for two metal mounted devices and a glass mounted devices measured in both forward (illuminated through the photoanode) and reverse (illuminated through the laminate counter electrode) illumination. Metal mounted devices incorporating a spin-coated c-TiO_2 layer exhibit significantly slower recombination than their glass counterparts. This is thought to be due to a secondary c-TiO_2 layer forming due to oxidation at the surface of the Ti foil during the thermal treatment of the substrate after the deposition of the c-TiO_2 precursor. This is reflected in the higher V_{OC} observed in metal-based devices over that of glass devices, fabricated at the same time and using the same materials. Proof that a thermally grown c-TiO_2 can act as an effective electron transport layer has been obtained by fabricating working devices on Ti foil, heat treated without prior deposition of a c-TiO_2 precursor. Although photovoltages are low in these devices due to very fast recombination (Fig. 4), these thermally grown c-TiO_2 layers were not optimised in any way leading to the possibility of effective c-TiO_2 layers being grown in *in situ* on Ti foils prior to deposition of the perovskite precursor solution.

Fig. 4 shows recombination data for two efficient metal mounted devices, one with an optimised PEDOT:PSS interlayer, and one with a thicker interlayer. It is interesting to note the increase the rate of recombination of the device with the thicker interlayer reflects the drop in voltage observed in Fig. 2 which we have attributed to degradation of the Spiro-OMeTAD. This degradation appears to have enabled faster recombination resulting in the lower voltages seen in Fig. 2 Since metal mounted devices are illuminated through the counter electrode (effectively in reverse) it is useful to compare with glass devices, also illuminated in reverse. The use of the transparent laminate provides an intriguing opportunity to measure the influence of reverse illumination whereby in a conventional cell architecture, incorporating an opaque Au contact, this is not possible. When comparing the recombination data of the same device illuminated from different sides it is interesting to note that recombination is slightly faster (for a given V_{OC}) when illuminating through the counter electrode side. This could indicate an additional interfacial recombination mechanism at the perovskite/HTM interface as, in reverse illumination, charge carriers are generated closer to the perovskite/HTM interface which could lead to an increased chance of recombination. However, since the TPV decays in these devices show monoexponential behaviour, it is likely that only one recombination mechanism dominates in these devices. Due to the order of magnitude difference in recombination lifetime between the device with the thermally grown c-TiO_2 layer and the device with the spin coated c-TiO_2 layer, it appears that interfacial recombination at the c-TiO_2/perovskite interface is the dominant recombination mechanism and so is a significant contributor to voltage losses in these devices. The small difference in recombination lifetimes observed when illuminating the FTO glass/laminate device from different directions is the subject of continuing research but may be due to the difference in electron and hole diffusion lengths reported elsewhere.[28]

In summary, we have demonstrated the first solution processed flexible organic-inorganic lead halide perovskite solar cells to be produced on a metallic foil substrate. Such devices have yielded PCEs of 10.3% and exhibit minimal performance degradation in spite of repeated bend cycles. A new PEDOT:PSS interlayer within the device has been optimised and was found to dramatically affect both the J_{SC} and fill factor of solar cells. In addition, we have identified by transient photovoltage decay, that recombination at c-TiO_2/perovskite

interface is the dominant recombination mechanisms in these devices, and have identified sources of optical attenuation as a result of the "reverse" illumination direction employed. Although this communication has focused on devices with a discretely deposited c-TiO_2 layer, there exists an exciting opportunity to optimise Ti foil devices with "self-grown" electron collection layers grown through thermally-induced oxidation of the substrate. Such devices would likely prove far easier to produce on a large scale due to the removal of a precision layer deposition step.

References

1 A. Kojima, K. Teshima, Y. Shirai and T. Miyasaka, *Journal of the American Chemical Society*, 2009, **131**, 6050–6051.
2 M. M. Lee, J. Teuscher, T. Miyasaka, T. N. Murakami and H. J. Snaith, *Science*, 2012, **338**, 643–647.
3 H.-S. Kim, C.-R. Lee, J.-H. Im, K.-B. Lee, T. Moehl, A. Marchioro, S.-J. Moon, R. Humphry-Baker, J.-H. Yum, J. E. Moser, M. Gratzel and N.-G. Park, *Sci. Rep.*, 2012, **2**, year.
4 *http://www.nrel.gov/ncpv/images/efficiency_chart.jpg*.
5 Z. Wei, K. Yan, H. Chen, Y. Yi, T. Zhang, X. Long, J. Li, L. Zhang, J. Wang and S. Yang, *Energy Environ. Sci.*, 2014, **7**, 3326–3333.
6 P.-Y. Chen, J. Qi, M. T. Klug, X. Dang, P. T. Hammond and A. M. Belcher, *Energy Environ. Sci.*, 2014, **7**, 3659–3665.
7 M. Liu, M. B. Johnston and H. J. Snaith, *Nature*, 2013, **501**, 395–398.
8 Q. Chen, H. Zhou, Z. Hong, S. Luo, H.-S. Duan, H.-H. Wang, Y. Liu, G. Li and Y. Yang, *Journal of the American Chemical Society*, 2014, **136**, 622–625.
9 J. Burschka, N. Pellet, S.-J. Moon, R. Humphry-Baker, P. Gao, M. K. Nazeeruddin and M. Gratzel, *Nature*, 2013, **499**, 316–319.
10 A. T. Barrows, A. J. Pearson, C. K. Kwak, A. D. F. Dunbar, A. R. Buckley and D. G. Lidzey, *Energy Environ. Sci.*, 2014, **7**, 2944–2950.
11 M. J. Carnie, C. Charbonneau, M. L. Davies, J. Troughton, T. M. Watson, K. Wojciechowski, H. Snaith and D. A. Worsley, *Chem. Commun.*, 2013, **49**, 7893–7895.
12 P. Docampo, J. M. Ball, M. Darwich, G. E. Eperon and H. J. Snaith, *Nat Commun*, 2013, **4**, 2761.
13 J. You, Z. Hong, Y. M. Yang, Q. Chen, M. Cai, T.-B. Song, C.-C. Chen, S. Lu, Y. Liu, H. Zhou and Y. Yang, *ACS Nano*, 2014, **8**, 1674–1680.
14 M. H. Kumar, N. Yantara, S. Dharani, M. Graetzel, S. Mhaisalkar, P. P. Boix and N. Mathews, *Chem Commun*, 2013, **49**, 11089–11091.
15 D. Liu and T. L. Kelly, *Nat Photonics*, 2014, **8**, 133–138.
16 J. W. Jung, S. T. Williams and A. K.-Y. Jen, *RSC Adv.*, 2014, **4**, 62971–62977.
17 B. J. Kim, D. H. Kim, Y.-Y. Lee, H.-W. Shin, G. S. Han, J. S. Hong, K. Mahmood, T. K. Ahn, Y.-C. Joo, K. S. Hong, N.-G. Park, S. Lee and H. S. Jung, *Energy Environ. Sci.*, 2015.
18 C. Roldan-Carmona, O. Malinkiewicz, A. Soriano, G. Minguez Espallargas, A. Garcia, P. Reinecke, T. Kroyer, M. I. Dar, M. K. Nazeeruddin and H. J. Bolink, *Energy Environ. Sci.*, 2014, **7**, 994–997.
19 L. Qiu, J. Deng, X. Lu, Z. Yang and H. Peng, *Angewandte Chemie International Edition*, 2014, **53**, 10425–10428.
20 S. Ito, N.-L. C. Ha, G. Rothenberger, P. Liska, P. Comte, S. M. Zakeeruddin, P. Pechy, M. K. Nazeeruddin and M. Gratzel, *Chem. Commun.*, 2006, 4004–4006.
21 D. Bryant, P. Greenwood, J. Troughton, M. Wijdekop, M. , M. Davies, K. Wojciechowski, H. J. Snaith, T. Watson and D. Worsley, *Advanced Materials*, 2014, **26**, 7499–7504.
22 J. M. Ball, M. M. Lee, A. Hey and H. J. Snaith, *Energy Environ. Sci.*, 2013, **6**, 1739–1743.
23 *E. Pat., EP2596509 A2, 2013*.
24 T. Leijtens, I.-K. Ding, T. Giovenzana, J. T. Bloking, M. D. McGehee and A. Sellinger, *ACS nano*, 2012, **6**, 1455–1462.
25 M. Carnie, T. Watson and D. Worsley, *International Journal of Photoenergy*, 2012, **2012**, 1–9.
26 P. R. F. Barnes, K. Miettunen, X. Li, A. Y. Anderson, T. Bessho, M. Gratzel and B. C. O'Regan, *Advanced Materials*, 2013, **25**, 1881–1922.
27 M. J. Carnie, C. Charbonneau, M. L. Davies, B. O. Regan, D. A. Worsley and T. M. Watson, *J. Mater. Chem. A*, 2014, **2**, 17077–17084.
28 S. D. Stranks, G. E. Eperon, G. Grancini, C. Menelaou, M. J. P. Alcocer, T. Leijtens, L. M. Herz, A. Petrozza and H. J. Snaith, *Science*, 2013, **342**, 341–344.